

# EFFECT OF CLADDING DIRECTION ON THE MICROSTRUCTURE AND MECHANICAL PROPERTIES OF HADFIELD GRADIENT LAYERS ON R260 RAILS

<sup>1</sup>Arman DADKHAH, <sup>1</sup>Eva SCHMIDOVA, <sup>1</sup>Filip KLEJCH, <sup>1</sup>Bohumil CULEK

<sup>1</sup>University of Pardubice, Faculty of Transport Engineering, Departments of Mechanics, Materials and Machine Parts, Pardubice, Czech Republic, EU, <u>arman.dadkhah@student.upce.cz</u>, <u>eva.schmidova@upce.cz</u>, <u>filip.klejch@upce.cz</u>, <u>bohumil.culek@upce.cz</u>

https://doi.org/10.37904/metal.2025.5138

#### **Abstract**

Rolling Contact Fatigue (RCF) is a critical issue that degrades rail surfaces, leading to structural damage and reducing service life. Effective repair techniques, such as plasma cladding with powder filler metal, can restore rail integrity and enhance performance. This study investigates the influence of cladding direction on the microstructure and mechanical properties of Hadfield gradient layers deposited on R260 rails. The research focuses on how deposition orientation affects hardness, phase transformations, and microstructural evolution, particularly the formation of martensitic layers and carbide precipitation within the heat-affected and repaired zones. Optical and electron microscopy are employed for microstructural analysis, while spherical indentation and Vickers hardness testing assess mechanical performance. The study reveals that cladding direction significantly influences carbide distribution, martensitic transformation, and hardness gradients, ultimately impacting fatigue resistance and durability. A deeper understanding of these variations provides valuable insights into optimizing cladding strategies for improved rail repair outcomes. The findings contribute to developing advanced repair methodologies, ensuring prolonged rail service life and enhanced resistance to fatigue-induced failures. Additionally, the study examines the effect of the number of welding layers and movement patterns of the welding torch in cladding to eliminate the need for post-weld heat treatment. This research serves as a foundation for refining welding parameters and deposition techniques to achieve superior mechanical performance in repaired railway components, ultimately leading to safer and more reliable railway infrastructure.

Keywords: Hadfield, plasma cladding, welding direction, martensite formation, indentation method

## 1. INTRODUCTION

Railway wheels are critical components in rail transport systems but are susceptible to various wear mechanisms, including adhesion wear, abrasion, and rolling contact fatigue. Improving fatigue resistance and achieving reliable weld repairs remain key engineering challenges. Among advanced repair techniques, plasma arc welding (PAW) with Hadfield steel—an austenitic manganese alloy known for its exceptional wear resistance, toughness, and strain hardening capacity—has emerged as a promising approach for surface cladding [1,2]. Surface cladding especially using plasma arc offers a concentrated and stable heat source (typically 10,000–16,000 K), compatibility with both wire and powder filler forms, and enhanced control over energy input, enabling superior bonding and mechanical performance compared to conventional welding processes such as GMAW and GTAW [3,4].

This study investigates the influence of torch movement patterns—specifically longitudinal and wave bead paths—on the deposition of Hadfield layers via PAW using powder filler metals. Various movement strategies have been shown to significantly affect weld quality and microstructure [5–8]. Through a comparative analysis of four sample sets, the effects on microstructural and mechanical properties were evaluated using optical



microscopy (OM), Scanning Electron Microscopy (SEM), EDS, and cyclic indentation testing to determine parameters such as yield strength and work hardening exponent (n-value). Emphasis was placed on understanding martensite formation and carbide precipitation, both of which adversely affect the dynamic durability of rails. The results aim to clarify key process-structure-property relationships to optimize repair strategies in railway applications.

## 2. EXPERIMENTAL PROCEDURES

Experiments were conducted on PAW specimens using argon as the shielding gas, with two torch movement patterns and different welding layers as variables. The PAW samples were divided into four sets: R1, R2, R3, and R4, all of which used powder filler metal. The R1 and R2 specimens consisted of a single weld metal (WM) layer applied using straight and box-type torch movement patterns, respectively. The same patterns were applied in R3 and R4, but with two WM layers, as shown in (**Figure 1**). The PAW process involved straight welding along eight lines to form a hard-faced layer in both R1 and R3. R260 rail steel was cut and machined to prepare the surfaces for weld bead deposition. **Table 1** presents the chemical compositions of the filler metal and the base metal (BM) before welding. The welding parameters (**Table 2**) were chosen to optimize the process and attain the desired material properties, with the heat input values determined based on BS EN 1011-1:2009. No preheating or post-welding thermal treatment was applied to the first layer to assess its suitability for rail applications. Interpass temperatures in R3 and R4 were monitored, and the second layer was welded at 140°C.

Table 1 Chemical analysis (wt.%)											
Elements	С	Si	Mn	Cr	Мо	Ni	Р	S	V	В	Fe
Base Metal	0.60- 0.80	0.10- 0.50	0.80- 1.30				≤ 0.040	≤ 0.040			5.
Filler Metal	0.44	0.48	14.4	14.1	0.39	1.31	0.016	0.003	0.18	<0.001	Balance

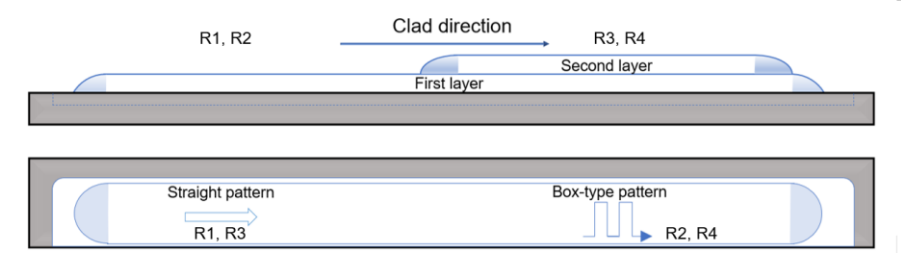


**Figure 1** Schematic illustration of the welding path and layer arrangement, showing the first and second layer deposition along the clad direction with straight and box-type patterns R1-R4

Welded run	Layer No.	Amperage	Voltage	Welding Speed
R1	1	147	30	(mm/s)
R2	1	96	26	3.5
	1	147	30	2.7
R3	2	147	30	5.0
R4 -	1	96	26	3.5
11.4	2	96	26	3.5

For microstructural analysis, the welded samples were prepared according to ASTM E3 standard practices. OM and SEM were employed to evaluate the etched surfaces. In addition, Vickers hardness testing was



conducted on the austenitic WM to characterize the hardness profile across the welded layers. Hardness measurements were performed under a load of 19.61 N with a dwell time of 12 seconds, following the ISO 6507-1 standard. Furthermore, spherical indentation tests were employed to evaluate key mechanical properties such as the yield strength and strain hardening exponent (n-value) of the weld layers. These tests were carried out using a 1 mm diameter ball indenter on a Zwick/Roell ZHU 2.5 testing machine. The procedure was performed following the ISO 6506-1 and ISO/TR 29381. Research by Okocha et al. [9] demonstrated that cyclic indentation applied to flat rail surfaces offers a reliable approach for estimating the yield strength. In this study, the following equations were applied to determine the local n-value and yield strength, based on the relationship between the maximum applied load and corresponding indentation depth:

$$\sigma = \frac{F_{\text{max}}}{\Psi * A(h_{\text{t}})} \tag{1}$$

$$A(h_c) = \pi (Dh_t - h_t^2)$$
(2)

$$\varepsilon = \xi \tan \theta$$
 (3)

In these expressions,  $\theta$  represents half of the contact angle, while A(h<sub>c</sub>) denotes the contact area corresponding to the maximum indentation depth (h<sub>t</sub>). The parameter  $\xi$  refers to the proportional constant associated with true strain, and  $\Psi$  represents the plastic constraint factor. For steel materials,  $\Psi$  is assigned a value of 3, and  $\xi$  is set to 0.14. Furthermore, d<sub>t</sub> refers to the measured indentation diameter, while D denotes the diameter of the ball indenter. Parameter A is a material-dependent constant, and m corresponds to Meyer's coefficient, as described in [10]. The constant value of 0.2285 applies specifically to carbon steels, though this value may vary for different materials [11].

$$d_t = 2\sqrt{(h_t D - h_t^2)} \tag{4}$$

$$F_{d_t^2} = A(d_t/D)^{m-2}$$
 (5)

$$\sigma_{\rm v} = 0.2285 * A$$
 (6)

## 3. RESULTS AND DISCUSSION

All welded specimens (see **Figure 2**) exhibited an austenitic microstructure within the welded metal zones, confirming the effectiveness of the welding parameters in achieving the desired phase composition. A smooth and homogeneous interface was observed, indicating good metallurgical bonding between the base and weld metals. The observations suggest that the wave box welding technique may offer improved reliability and defect-free joints compared to the straight-line approach, especially in the initial stages of the weld where thermal and mechanical conditions are critical.

Microscopic observations revealed notable differences in the microstructure of the clad layers depending on the cladding direction. The Heat-Affected Zone (HAZ) in all samples exhibited clear signs of reheating leading to the reheating to austenite, including partial austenite reformation and carbide dissolution near the fusion boundary. The martensitic transformation was evident in localized regions, particularly beneath the fusion line, where high cooling rates facilitated the formation of lath martensite. The use of the wave box welding pattern resulted in a significantly lower extent of martensite formation compared to longitudinal welding.

Energy-Dispersive Spectroscopy (EDS) analysis of the weld metal of R1 and R3 revealed a sulfur-rich phase located explicitly along grain boundaries. These inclusions contained Cr (wt.% 29.8), V (wt.% 1.0), Fe (wt.% 46.2), and Mn (wt.% 21.4), suggesting the formation of sulfur-based complex phase during solidification. Their intergranular positioning is critical, as it indicates element segregation connected with the high heat input during PAW. Such inclusions compromise grain boundary cohesion and act as stress concentrators, particularly under cyclic mechanical loading. This microstructural feature may lower the resistance of the welded layer to RCF and promote premature crack initiation. Consequently, strict control of sulfur content and



a refined understanding of filler/BM interactions are essential for optimizing weld performance. Carbide precipitation, identified as (Fe-Mn)<sub>3</sub>C was more pronounced in samples clad in the transverse direction, suggesting differential thermal histories across the cladding orientations [12].

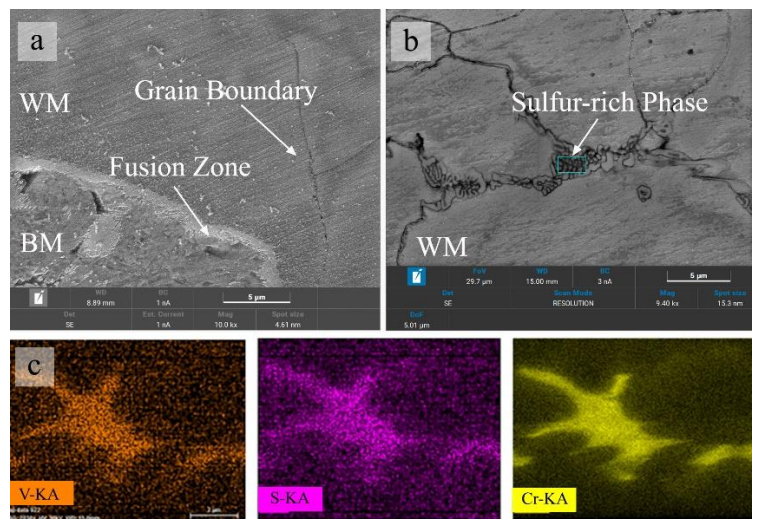


Figure 2 Optical micrographs of (a) R1, (b) R3, (c) R3 EDS analysis

Hardness profiles across the cross-section are depicted in (**Figure 3**) showed a hardness profile linked to the cladding direction and number of the layers. Samples clad in R2 exhibited a smoother transition in hardness from the fusion zone to the substrate, with peak hardness values around 430 HV near the surface, gradually decreasing into the base rail. In contrast, the longitudinal clad samples displayed steeper gradients, with peak values reaching 550 HV near the clad-HAZ interface. Adding a second layer in R4 specimens, created a noticeable variation in the clad-HAZ interface. The higher localized hardness is attributed to increased martensite, bainite content, and refined microstructure caused by directional heat flow and solidification front disruption.

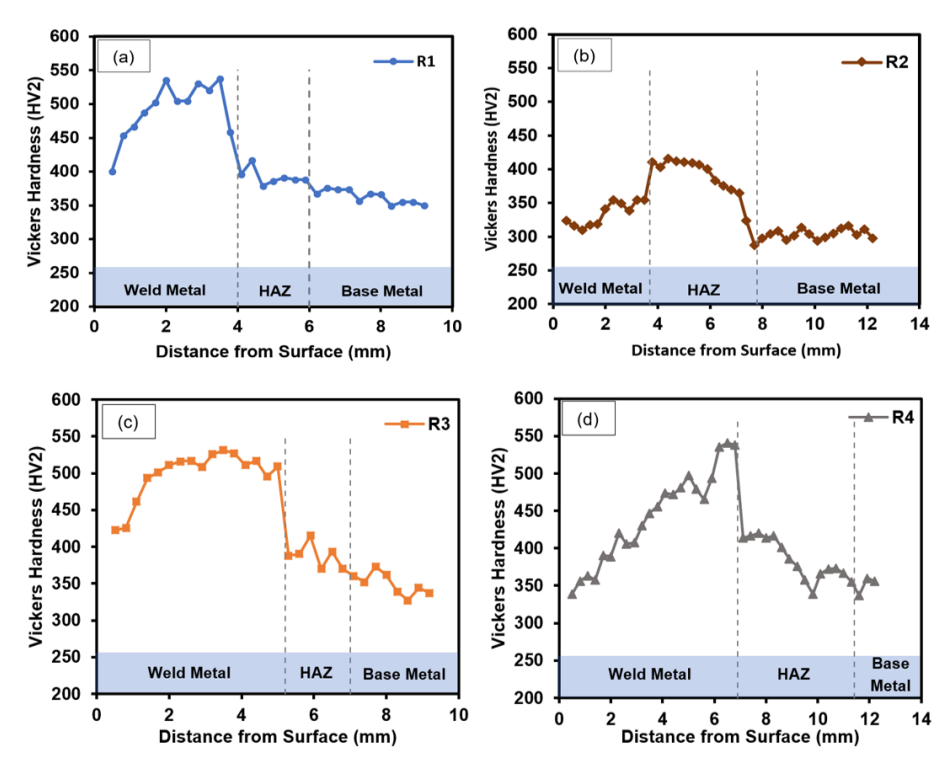


Figure 3 Hardness profile measurements of (a) R1, (b) R2, (c) R3, and (d) R4



Spherical indentation testing confirmed that variations in the welding pattern had no statistically significant effect on the mechanical response of the welded layer. In contrast, the application of a second layer led to a marginal reduction in both the yield strength and the work hardening exponent (n-value) across all samples. The corresponding values of mechanical properties, derived from the load-displacement curves, are summarized in **Table 3**.

Directional solidification was instrumental in regulating thermal gradients, thereby influencing carbide precipitation zones, and the extent of martensitic transformation. The application of longitudinal welding facilitated more uniform thermal dissipation, mitigating residual stress accumulation and reducing susceptibility to solidification cracking. Additionally, the wave-box torch pattern suppressed localized hardness maxima, thereby minimizing the risk of embrittlement. Although the terminal austenitized region within the HAZ typically undergoes martensitic transformation upon cooling, the implementation of combined longitudinal and wave-box welding strategies shows potential for reducing this transformation, warranting further experimental validation.

Welded Run Layer No.		Indentation Yield Strength (MPa)	n-Value	
R1	1	528.36	0.39	
R2	1	600.40	0.33	
R3	1	514.60	0.24	
KS	2	459.23	0.22	
D/	1	501.05	0.39	
R4	2	492.80	0.19	

#### 4. CONCLUSION

This study successfully demonstrated the feasibility and effectiveness of the plasma arc welding method using Hadfield weld metal produced from powder filler material. Comprehensive experimentation and analysis confirmed that the selected parameters significantly affect weld quality, mechanical properties, and the overall performance of the welded joints. The findings indicate that optimization of key process variables such as heat input, welding speed, and electrode configuration, can enhance structural integrity and productivity. Martensite formation in the HAZ was significantly reduced when the wave-box welding pattern was employed, compared to longitudinal welding. Additionally, the cyclic indentation testing method proved to be a practical and reliable approach for evaluating variations in yield strength and the work hardening exponent of the welded material. The wave-box pattern exhibited grain boundaries free of sulfur-rich phases, which can be attributed to the welding process and heat distribution during solidification.

## **ACKNOWLEDGEMENTS**

This work was supported by the project no. SGS\_2025\_008 - Current Aspects in the Field of Transport Vehicles and Infrastructure at the Faculty of Transport Engineering, University of Pardubice. The authors gratefully acknowledge this support.

#### **REFERENCES**

- [1] C. EFSTATHIOU, H. SEHITOGLU, Strengthening Hadfield steel welds by nitrogen alloying, Materials Science and Engineering: A 506 (2009) 174–179. <a href="https://doi.org/10.1016/j.msea.2008.11.057">https://doi.org/10.1016/j.msea.2008.11.057</a>.
- [2] U. GÜROL, E. KOCAMAN, Effect of Different Heat Treatment Procedures on the Corrosion Behavior of High-Manganese Austenitic Steels, International Journal of Metalcasting (2025). https://doi.org/10.1007/s40962-024-01543-x.



- [3] K. SHARMA, A Review on Cladding Process to Improve Metal Properties, Int J Res Appl Sci Eng Technol 6 (2018) 3125–3130. https://doi.org/10.22214/ijraset.2018.4520.
- [4] X. SHI, Y. LIU, M. ZHANG, Z. SUN, Dual-constricted plasma arc cladding of Inconel 625 alloy: arc characteristics, microstructure, and corrosion resistance, Journal of Materials Science: Materials in Engineering 20 (2025). <a href="https://doi.org/10.1186/s40712-025-00262-3">https://doi.org/10.1186/s40712-025-00262-3</a>.
- [5] A.I. ALBANNAI, A.J. RAMIREZ, The effect of altering heat input & torch motion on the grain formation of SS316L material in WAAM, Discover Mechanical Engineering 3 (2024). <a href="https://doi.org/10.1007/s44245-024-00082-3">https://doi.org/10.1007/s44245-024-00082-3</a>.
- [6] L. CHEN, G. LIU, S. LI, Y. MO, Z. HAN, X. LIANG, H. PAN, A novel 8-shape trajectory weaving welding control algorithm with auto-adjust welding torch attitude, International Journal of Advanced Manufacturing Technology 120 (2022) 8377–8387. https://doi.org/10.1007/s00170-022-09225-w.
- [7] Kalyankar VIVEK, Bhoskar AVISHKAR, Influence of torch oscillation on the microstructure of Colmonoy 6 overlay deposition on SS304 substrate with PTA welding process, Metall. Res. Technol. 118 (2021) 406. https://doi.org/10.1051/metal/2021045.
- [8] J. HUANG, F. LI, C. SHEN, Y. ZHANG, J. XIN, G. RUAN, X. HUA, Optimization of shape-forming accuracy in arc-striking and arc-extinguishing areas of weld bead by torch hovering for directed energy deposition-arc manufactured nickel aluminum bronze alloy component, International Journal of Advanced Manufacturing Technology 131 (2024) 3957–3973. https://doi.org/10.1007/s00170-024-13210-w.
- [9] S.I. OKOCHA, F. YU, P.Y.B. JAR, M.T. HENDRY, Indentation Testing Method for Determining Mechanical Properties and Tensile Flow Curve of High-Strength Rail Steels, Exp Mech 63 (2023) 839– 852. <a href="https://doi.org/10.1007/s11340-023-00939-w">https://doi.org/10.1007/s11340-023-00939-w</a>.
- [10] K. SHARMA, P.K. SINGH, V. BHASIN, K.K. VAZE, Application of Automated Ball Indentation for Property Measurement of Degraded Zr2.5Nb, 2011.
- [11] United States Patent (19) Haggag 54 FIELD INDENTATION MICROPROBE FOR, n.d.
- [12] A. DUMAY, J.-P. CHATEAU, S. ALLAIN, S. MIGOT, O. BOUAZIZ, Influence of addition elements on the stacking-fault energy and mechanical properties of an austenitic Fe–Mn–C steel, Materials Science and Engineering: A 483 (2008) 184–187.